Lab on a Chip

Devices and applications at the micro- and nanoscale

Accepted Manuscript

Volume 17
Number 1
7 January 2017
Pages 1-200

Lab on a Chip

Devices and applications at the micro- and nanoscale

rsc.li/loc

ISSN 1473-0197

ROYAL SOCIETY OF CHEMISTRY

PAPER
Chengzhi Hu, Bradley J. Nelson et al.
Characterization of size-dependent mechanical properties of top-growing cells using a lab-on-a-chip device

This is an Accepted Manuscript, which has been through the Royal Society of Chemistry peer review process and has been accepted for publication.

Accepted Manuscripts are published online shortly after acceptance, before technical editing, formatting and proof reading. Using this free service, authors can make their results available to the community, in citable form, before we publish the edited article. We will replace this Accepted Manuscript with the edited and formatted Advance Article as soon as it is available.

You can find more information about Accepted Manuscripts in the Information for Authors.

Please note that technical editing may introduce minor changes to the text and/or graphics, which may alter content. The journal's standard Terms & Conditions and the Ethical guidelines still apply. In no event shall the Royal Society of Chemistry be held responsible for any errors or omissions in this Accepted Manuscript or any consequences arising from the use of any information it contains.

ROYAL SOCIETY OF CHEMISTRY

rsc.li/loc

1   **HiPSC-derived multi-organoids on chip system for safety assessment of**

2   **antidepressant drug**

3   Fangchao Yin, [a,d,1] Xu Zhang, [a,1] Li Wang, [e] Yaqing Wang, [a,d] Yujuan Zhu, [a,d]

4   Zhongyu Li, [a] Tingting Tao, [a,d] Wenwen Chen, [a,d] Hao Yu, [a] and Jianhua Qin[*a,b,c,d]

5   [a] CAS Key Laboratory of SSAC, Department of biotechnology, Dalian Institute of

6   Chemical Physics, Chinese Academy of Sciences.

7   [b] Institute for Stem Cell and Regeneration, Chinese Academy of Sciences, Beijing,

8   China.

9   [c] CAS Center for Excellence in Brain Science and Intelligence Technology, Chinese

10   Academy of Sciences, Shanghai, China.

11   [d] University of Chinese Academy of Sciences, Beijing, China.

12   [e] Institutes of Biomedical Sciences, Fudan University, Shanghai, China.

13   [1] These authors contribute equally to the work.

14   * Corresponding author: Prof. J. Qin, E-mail: jhqin@dicp.ac.cn

15   **Abstract**

16   The poor predictive power of the existing preclinical models has spurred efforts to

17   develop human relevant models for accurate assessment of drug safety. In this work,

18   we developed a multi-organoids-on-a-chip system derived from human induced

19   pluripotent stem cells (hiPSCs), which allows for the assessment of the cardiac safety

20   of antidepressant drug, following liver metabolism *in vitro*. This liver-heart organoids

21   on chip device contains compartmentalized chambers separated by porous membrane,

22   which permits the co-culture of 3D human liver organoids (LOs) in the upper

23   multi-well chamber and cardiac organoids (COs) in the bottom micropillar array

24   simultaneously. The co-cultured liver and heart organoids on chip maintained good

25   viability and human organ-specific functions respectively, including the synthesis of

26   albumin and urea of liver organoids, and beating function of cardiac organoids. In

27   particular, the liver organoids displayed proper metabolic capabilities with high

28   expression of CYP450 enzyme genes. Clomipramine, a widely used antidepressant

29   drug, can be metabolized into the active metabolite (desmethylclomipramine) through

30 the hepatic CYP450 enzymes of liver organoids on chip identified by mass

31 spectrometry. After exposure to 1 μM clomipramine in the liver chamber for 24h and

32 48h, the co-cultured heart organoids in the bottom layer showed significantly reduced

33 cell viability, impaired functions of cardiac beating and calcium flux, indicating the

34 hepatic metabolism dependent cardiotoxicity induced by clomipramine. By

35 combining stem cell biology and microengineered technology, this proposed

36 hiPSC-derived multi-organoids chip system can reflect human organ-specific

37 functions, as well as the complex process of drug metabolism and responses at the

38 multi-organ level. It may provide a novel platform for the assessment of drug

39 effectiveness and safety *in vitro*.

40

41 **Keywords:** Clomipramine, human induced pluripotent stem cell,

42 multi-organoids-on-chip, drug metabolism, heart-liver chip

43

44 **1. Introduction**

45 Medications present safety challenges because it needs to balance the well-being of

46 patients with potential side effect of drugs[1, 2]. Generally, only 5 in 10000 compounds

47 can enter into the clinical trails and eventually 1 of them is approved by the Food and

48 Drug Administration (FDA)[3, 4]. Drug-induced hepatic and cardiac side effects are

49 main concerns for drugs failure from clinical trails and withdrawn from the market[5, 6].

50 The models that can accurately predict human outcomes of drug toxicity and the

51 crosstalk between different organs are still lacking. Thus, the assessment of drug

52 safety in a physiologically relevant manner may greatly contribute to guide the

53 clinical usage of medications.

54 *In vivo,* the pharmacokinetic process of drugs involves in absorption, distribution,

55 metabolism and exclusion. Liver as a major organ of drug metabolism, greatly

56 determines pharmacological properties of drugs, such as the bioavailability and

57 adverse effects. Gain insight into the drug metabolism and safety may greatly

58 contribute to increase the success rate of drug discovery and guide the clinical usage

59   of medication. However, the traditional preclinical models mainly rely on the

60   two-dimensional (2D) monolayer cell cultures and animal experiments. Generally, the

61   monolayer cell cultures are oversimplified to reflect the physiological conditions and

62   xenobiotic metabolism of organs *in vivo*. Moreover, the single cell type cannot model

63   the physiological complexity of inter-organ interactions and the process of drug

64   pharmacokinetics. Although the *in vivo* animal models have been applied to assess the

65   safety of antidepressants, they can hardly represent the human relevant responses to

66   drugs due to the interspecies divergence[7]. Therefore, it is highly desirable to develop

67   human relevant model *in vitro* for safety assessment of antidepressant.

68   Organoids are 3D cellular clusters by self-organization of pluripotent stem cells

69   (PSCs) *in vitro* that are capable of recapitulating key features of native organs or

70   tissues[8, 9]. Especially, human induced PSC (hiPSC)-derived organoids hold great

71   potential for organ development studies, disease modeling and drug testing.

72   Organoids-on-chip is emerging as an innovative technology by combining

73   self-organized organoids and organs-on-chips to build higher-fidelity 3D organ

74   models[10-13], thus potentially bridging the gap between monolayer cultures and animal

75   models. The integrative strategies could be used for better produce the *in vitro* human

76   organ models by precise control over the 3D culture, dynamic flow and mechanical

77   cues in an organ chip device[14-16]. Recently, a series of organoid-on-a-chips have been

78   successfully established, such as liver[17], brain[12], and islet[18] etc. The

79   organoid-on-a-chip platform offers new frontiers and possibilities for applications in

80   biomedicine.

81   In this work, we build a multi-organoids-on-chip system from hiPSCs for the

82   safety assessment of antidepressant drug, for the first time. Clomipramine, a kind of

83   FDA-approved tricyclic antidepressants for patients with severe depression[19, 20], was

84   used as a model drug in this system. The bioengineered organoids chip system was

85   designed with four layers that allowed the 3D co-culture of liver and heart organoids

86   within the compartmentalized chambers after the formation of self-organized

87   organoids from hiPSCs. The upper multi-well chamber allows the culture of liver

88 organoids for the metabolism of clomipramine, and the bottom micropillar array

89 permits the differentiation and culture of heart organoids for the assessment of drug

90 toxicity. The organ-specific genes expression and functions of the liver and cardiac

91 organoids were identified in the co-culture system. Then the responses of heart

92 organoids to clomipramine were investigated by examining the cardiac viability and

93 functions in the presence and absence of hepatic metabolism. This human

94 multi-organoids system derived from hiPSCs may provide a proof-of-concept for drug

95 safety assessment in a physiologically relevant manner.

96 **2. Materials and methods**

97 **2.1 Design and fabrication of multi-organoids on chip device**

98 The device was fabricated using soft lithography techniques as previously

99 described[21, 22]. The device consisted of four layers: a top layer, a

100 ploy(dimethylsiloxane) (PDMS, Dow corning, USA) layer with 500 μm diameter

101 through-hole, a transparent polycarbonate porous membrane with 0.4 μm pores

102 (Whatman Corp, United Kingdom) and a bottom layer (**Fig. 1**). The top PDMS layer

103 was fabricated with a culture channel (length: 15 mm, width: 5 mm and height: 1

104 mm). The bottom PDMS layer (length: 20 mm, width: 5 mm and height: 1 mm)

105 consisted of an array of patterned micropillars (diameter: 500 μm and height: 700 μm)

106 with gaps of 100 μm use for 3D culture of cardiac organoids. The three PDMS layers

107 were generated by mixing the PDMS at weight ratio of 10:1 and curing at 80 ℃ for 30

108 min. The top PDMS layer was bonded to the through-hole PDMS membrane

109 following oxygen plasma treatment. The polycarbonate porous membrane adhered to

110 the surface of the bottom layer through the electrostatic interaction, then PDMS

111 pre-polymer was smeared on the membrane. After curing, the through-hole PDMS

112 membrane and transparent membrane were bonded together following the plasma

113 treatment. Before the experiments, the chip devices were sterilized in an autoclave.

114 **2.2 HiPSCs culture**

115 The hiPSC line was kindly provided by Dr. Ning Sun[23, 24]. Undifferentiated

116 hiPSCs were cultured in mTeSR1 medium (STEMCELL Technologies, Canada) on

117   Matrigel (1:50 dilution, BD Bioscience, USA)-coated feeder-free 6-well plates

118   (Guangzhou Jet Bio-Filtration Co., Ltd.). The medium was changed daily until the

119   cells reached approximately 80 % to 90 % confluence. Cells were then dissociated

120   using Accutase (Sigma, USA) and passaged at 1:5 ratio. To promote the viability of

121   hiPSCs, mTeSR1 medium contained 10 μM Y27632 (ROCK inhibitor, STEMCELL

122   Technologies, Canada) was used for cell culture for the first 1 h and then the medium

123   was replaced by fresh mTeSR1 medium without Y27632.

124   **2.3 Differentiation of liver organoids from hiPSCs**

125   The hiPSCs were differentiated into liver organoid according to the approaches

126   reported previously[17, 25]. Briefly, the hiPSCs ($\sim 5 \times 10^6$) were resuspended and

127   dissociated into small pieces to generate uniform embryoid bodies (EBs) in mTeSR1

128   medium with 10 μM Y27632. To generate liver organoid, the medium was changed to

129   RPMI 1640 medium (Invitrogen, USA) supplemented with 1% knockout serum

130   replacement (KSR, Gibco, USA), 1% B27 supplement (50 × , Gibco, USA), 1%

131   GlutaMAX (Invitrogen, USA), 1% penicillin-streptomycin (Beyotime, China). For

132   endoderm differentiation, activin-A (100 ng mL^{-1}, PeproTech, USA) was added to the

133   medium for the first 5 days. From day 5 to 10, HGF (20 ng mL^{-1}, PeproTech, USA)

134   and bFGF (10 ng mL^{-1}, PeproTech, USA) were added to the medium for the

135   differentiation and expansion of hepatic progenitors in organoids. From day 10 to 15,

136   the medium was changed to HCM medium (ScienCell, USA) consisting of

137   dexamethasone (10^{-7} M, Sigma-Aldrich, USA) and oncostatin M (OSM, 10 ng mL^{-1},

138   R&D, USA) to promote further hepatocyte maturation. After day 15, the liver

139   organoids were cultured in HCM medium supplemented with 10^{-7} M dexamethasone

140   for all the following experiments.

141   **2.4 Differentiation of cardiac organoids from hiPSCs**

142   To generated cardiac organoids, the dissociated hiPSCs ($\sim 5 \times 10^6$) were

143   resuspended in mTeSR1 medium containing 10 μM Y27632 and seeded on the

144   bottom channel (the gap between transparent membrane and bottom layer) to form

145 EBs. On day 0, the EBs were induced in RPMI 1640 medium adding with B27 minus

146 insulin (50×, Gibco, USA) and glycogen synthase kinase 3 inhibitor CHIR99021 (12

147 μM, Selleck, USA). After 24 h, the medium was replaced with fresh RPMI 1640

148 medium containing B27 minus insulin. After 2 more days incubation, the medium was

149 changed to RPMI 1640 medium with B27 minus insulin and Wnt inhibitor IWP2 (5

150 μM, Selleck, USA). On day 5, the culture medium was replaced with fresh RPMI

151 1640 medium with B27 minus insulin. On day 7, the cells were fed with RPMI 1640

152 medium containing B27 every 3 days. The beating cardiac organoids were observed at

153 day 10-12 after differentiation.

154 **2.4 Integration of liver and heart organoids on chip**

155 The cardiac organoids were induced and grown in the bottom chamber of the chip

156 for 20 days. The liver organoids were then seeded into the upper culture chamber. The

157 medium was mixed at a ratio of 1:1 with RPMI 1640 medium containing B27 and

158 HCM medium supplemented with 10^{-7} M dexamethasone, which was changed every

159 day. After co-culturing for 7 days, clomipramine at different concentrations was

160 added to the upper liver culture chamber for 24 h and 48 h.

161 **2.5 Beating analysis of cardiac organoids**

162 The beating of cardiac tissue was recorded by real time video recording with a

163 high-resolution CCD (Leica, Germany). Videos of beating cardiac organoids were

164 then analyzed using motion tracking software as described before[26, 27]. Briefly, these

165 beating cardiac organoids videos were transformed into a series of single-frame image

166 files (10 frames/s) and then input to motion tracking software[26] for calculation.

167 **2.6 Immunocytochemistry**

168 Liver organoids and cardiac organoids for immunostaining were prepared as

169 described in our previous work[17, 28]. Briefly, organoids were fixed with 4%

170 paraformaldehyde for 20 min at room temperature. The fixed organoids were

171 dehydrated by incubation with 30% sucrose solution overnight at 4 ℃. Organoids

172 were embedded in O.C.T. compound (Sakura) and cryosectioned at 10 μm with a

173 cryostat (Leica). The freezing sections were washed with PBS to remove excess

174   O.C.T. and permeabilized with 0.25% Triton X-100 for 10 min. Sections were

175   blocked with goat serum (Solarbio, SL1) for 1h at room temperature, and then

176   incubated with primary antibodies overnight at 4℃. Samples were washed with PBS

177   three times and were then incubated with secondary antibodies for 1 h at room

178   temperature. The fluorescent images were recorded using a confocal microscope

179   (Olympus). Primary and secondary antibodies used here were listed in the **Table S1**.

180   **2.7 Real-time PCR**

181   The real-time PCR was performed as described in our previous study[11]. Briefly,

182   the total RNA was extracted from the organoids or hiPSCs using Trizol reagent

183   (TAKARA).   Then, the RNA was reverse-transcribed to generate cDNA with

184   PrimeScript RT Reagent Kit (Takara) and the concentrations of the RNA were

185   measured by a NanoDrop spectrophotometer (Thermo, America) to ensure that we

186   used same mass of mRNA (250 ng/ml) in each sample before the reverse

187   transcription. Finally, quantitative PCR (qPCR) was performed on PikoReal 96

188   real-time PCR System (Thermo). The housekeeping gene (β-actin) was used as an

189   internal control for normalization of all qPCR results. Primers were listed in **Table**

190   **S2**.

191   **2.8 Cell viability analysis**

192   Cell viability of human liver and heart organoids were examined after the

193   incubation with 1 μM or 10 μM clomipramine for 24 h and 48 h using the CCK-8 kit

194   (Cell Counting Kit-8, Dojindo). The experiments have been performed according to

195   the manufacturer's instructions.

196   **2.9 Urea synthesis**

197   The media from the supernatant of liver organoids on chip were collected for urea

198   measurement. The concentration of urea production in the medium was measured

199   using a QuantiChrom urea assay kit (BioAssay Systems) according to the

200   manufacturer.

201   **2.10 Calcium imaging**

202   After the drug treatment, cardiac organoids were incubated with Fluo-4 Direct^{TM}

203 Calcium reagent (Invitrogen) at 37 °C for 60 min. Afterwards, the reagent was

204 removed and changed to RMPI 1640 medium. The videos of calcium sparks were

205 recorded using a high-resolution CCD. Then the videos were exported as a series of

206 PNG files for beating study using Adobe Premier Pro2017. The PNG files were

207 analyzed using image-Pro Plus software to detect the fluorescence intensity changing

208 over time as previously described[29]. $\Delta F/F0$ was calculated to normalize differences of

209 the indicator concentration between cells.

210 **2.11 Drug metabolite analysis using LC-MS (Liquid chromatography mass**

211 **spectrometry)**

212 The stock solution of 10 mM clomipramine (clomipramine HCl, Selleck

213 Chemicals) was prepared in H_2O. After 7 days of co-culture, 1 μM clomipramine was

214 added to the medium in the upper chamber and metabolized for 24 h. Then, 500 μL of

215 the supernatant was collected from the chamber and added to 100 μL acetonitrile and

216 500 μL sodium carbonate solution (1 mol L^{-1}), followed by mixing. The mixture was

217 added to 3 mL n-hexane and then vortexed for 1 min, reciprocated for 15 min. After

218 centrifuging at 4000 rpm for 15 min, the organic phase was transferred to a

219 polyethylene tube and dried in a vacuum desiccator. The dried residue was

220 re-dissolved in 200 μL acetonitrile and detected using an Agilent Ultra High

221 Performance Liquid Chromatography-Mass Spectrometer (LC-MS, Agilent 1290

222 Infinity, 6540 UHD Q-TOF). Finally, 20 μL aliquots was injected into LC-MS for

223 analysis of the drug metabolites.

224 **2.12 Statistical analysis**

225 All quantitative data were calculated from three independent experiments.

226 Statistical significance was analyzed using Student's *t*-test and present as mean±SD. *

227 $P < 0.05$, ** $P < 0.01$, ***$P < 0.001$ were determined to be significant.

228 **3. Results and discussion**

229 **3.1 The design and operation of the multi-organoids-on-chip**

230 In this study, we designed and fabricated a multi-organoids-on-chip device, which

231 enabled to evaluate the drug-induced cardiac toxicity after its metabolism in liver

232　organoids (**Fig. 1**). This liver-heart organoids-on-chip device contains four layers,

233　including the top layer, through-hole PDMS layer, polycarbonate porous membrane

234　and bottom layer. The through-hole PDMS layer and the polycarbonate membrane

235　formed the upper microwell chamber, which permitted the 3D culture of

236　hiPSC-derived liver organoids. The bottom chamber with micropillar array allowed

237　the controlled formation of EBs with consistent morphology, in situ differentiation

238　and self-organization of heart organoids from hiPSCs. The microwell and micropillar

239　structures facilitate the production of uniform organoids and avoid the fusion of

240　organoids, thus reducing their variability. Moreover, the compartmentalized chip

241　design is flexible and conductive to different ways of drug administration, organoids

242　collection and downstream analysis. It is noted, the polycarbonate porous membrane

243　sandwiched between the upper and lower layers can not only facilitate the

244　interconnection of the media, drug metabolites diffusion and nutrients exchange, but

245　also be amenable to real-time imaging of organoids on chip. As such, the established

246　multi-organoids-on-chip is feasible to be applied for the subsequent co-culture of

247　distinct organoids and the assessment of drug bioactivity and toxicity via organ-organ

248　interactions.

249　**3.2 Functional characterization of hiPSC-derived liver and cardiac organoids**

250　To generate 3D cardiac organoids from hiPSCs on a chip, we used a defined

251　differentiation protocol with chemicals and growth factors added into the medium.

252　The hiPSC-derived EBs were initially generated on the micropillar array of bottom

253　layer, following in situ sequential induction of the mesendoderm, cardiac specific

254　mesoderm, cardiomyocytes and organization of cardiac organoids (**Fig. 2a and S1**).

255　Generally, the spontaneous contraction occurs at day 10 to day 12 after

256　differentiation. To evaluate the features of cardiac organoids differentiation, we

257　examined the expression of cardiac-specific genes by real-time PCR (**Fig. 2b**). As

258　expected, the expression of cardiac-specific markers (cTnT and TNNT3) significantly

259　increased on day 20 compared to the hiPSC control, while the expression of the

260　pluripotent markers of stem cells decreased **(Fig. S1b)**. Moreover, the expression of

261 cardiac transcriptional factor (NKX2.5) was detected at markedly high levels in heart

262 organoids. To further identify the maturity of cardiac organoids, the

263 immunohistochemical analysis of cardiac-specific markers was performed in

264 organoids (**Fig. 2c**). The results showed an abundant expression of cTnT in cardiac

265 organoids on day 20. These data validated the efficient differentiation of cardiac

266 organoids from hiPSCs in our device.

267 The liver organoids were generated from hiPSC-derived EBs, followed by

268 endoderm differentiation, hepatic progenitor induction and maturation using a

269 three-stage differentiation protocol (**Fig 3a and S2**). To examine the differentiation of

270 liver organoids, the expressions of pluripotent markers of stem cells and hepatic

271 lineage markers were tested by real-time PCR. The expression of pluripotent markers

272 (OCT4 and NANOG) decreased **(Fig. S2b)**, which suggests the differentiation of

273 hiPSCs. While the hepatic progenitor (AFP) and mature hepatocyte (ALB and

274 HNF4α) markers were significantly upregulated in liver organoids on 20 days of

275 differentiation (**Fig. 3b**). Moreover, the immunohistochemical analysis showed a

276 higher expression of ALB and cytochrome P450 (CYP3A4) in organoids on day 20

277 **(Fig. 3c)**, indicating the representative metabolic function of the liver organoids.

278 These results suggested the efficient differentiation of hiPSCs into hepatic lineages

279 and the formation of liver organoids.

280 **3.3 Co-culture of liver and cardiac organoids on chip**

281 Multi-organs-on-chip system enables the modeling of the crosstalk among organs,

282 holding great potential to investigate the systemic diseases and pharmacology. To

283 evaluate the cardiac safety of antidepressants administration following liver

284 metabolism, we integrated the liver and cardiac organoids on a multilayered chip

285 device to enable the co-culture of these organoids. The cardiac organoids were

286 differentiated from hiPSCs in the bottom layer of the device for 20 days, then liver

287 organoids were infused into the upper chamber. To verify the feasibility of the

288 integrated microphysiological system, the functional characterizations of the

289 co-cultured human cardiac and liver organoids were identified. At first, the urea

290   production of liver organoids in the co-culture system was examined to assess the

291   liver-specific function. As shown in **Fig. 4a,** urea production was markedly increasing

292   at day 3 and 7 of co-culture. Moreover, the liver organoids exhibited significantly

293   increased expressions of liver-specific CYP450 enzyme genes (CYP3A4 and

294   CYP1A2) on day 7. The expressions of other metabolic enzyme genes, such as

295   CYP2C19 and CYP2D6, in liver organoid co-cultured with cardiac organoid were

296   similar to that in liver organoid cultured alone (**Fig. 4b**). These data suggested that

297   liver organoids displayed favorable specific functions in this integrated system.

298   In addition, the cardiomyocytes specific functions including beating rate and

299   velocity were measured in cardiac organoids from day 1 to day 7 in the presence or

300   absence of liver organoids. As shown in **Fig. 4c** and **4d**, the cardiac organoids in

301   co-culture system displayed no significant differences in terms of spontaneous beat

302   frequency and maximum beating velocities in comparison with single cultures.

303   Compared with previous work that reported the increasing heart rate when co-culture

304   with hepatocytes[30], the stable functions of cardiac tissue here may benefit from the 3D

305   structure of organoid, which is more physiological morphology. Besides, the

306   organoids in the chip exhibited good uniformity that could increase the stability of

307   functions as well. Overall, cardiac and liver organoids maintained their tissue-specific

308   functions in the co-culture system over 7 days, reflecting that this *in vitro* liver-heart

309   model could might be available to assess drug cardiotoxicity following liver

310   metabolism.

311   **3.4 Identification of clomipramine metabolite in the multi-organoids on chip**

312   Liver plays a crucial role in the substance metabolism and detoxification *in vivo*.

313   CYP450 enzymes are vital drug metabolizing enzymes in human liver. Four typical

314   cytochrome enzymes, CYP1A2, CYP2C19, CYP2D6 and CYP3A4, have been found

315   to be closely related to the clomipramine metabolism[31] (**Fig. 5a**). Specifically,

316   clomipramine is hydroxylized to hydroxyclomipramine by CYP2D6, then

317   demethylated to desmethylclomipramine by CYP2C19, CYP3A4, and finally

318   converted to hydroxydesmethylclomipramine by CYP2D6. To assess the metabolic

319 capacity of liver organoids, we examined the expression of CYP1A2, CYP2C19,

320 CYP2D6 and CYP3A4 using real-time PCR. As shown in **Fig. 5b**, all four drug

321 metabolism-related CYP450 enzymes were significantly upregulated in the liver

322 organoids on day 20, demonstrating the potential metabolic capacity of liver

323 organoids. Furthermore, to verify the drug metabolism by the liver organoids, 1 μM

324 clomipramine was introduced to the liver organoids for 24 h. Then the supernatant

325 was collected to identify the production of metabolites with LC-MS/MS. As shown in

326 **Fig. 5c-d**, clomipramine with m/z 315 and desmethylclomipramine with m/z 301

327 were detected (top of **Fig. 5c-d**). Notably, the peak of desmethylclomipramine (m/z

328 301) was observed only in the spectrogram after its metabolism in liver organoids

329 (**Fig. S3**). Moreover, the characteristic peaks of secondary mass spectrograms (bottom

330 of **Fig. 5c-d**) double confirmed the presence of these two compounds. These data

331 suggested that hiPSC-derived liver organoids possessed the metabolic ability to

332 metabolize clomipramine into desmethylclomipramine, which accurately

333 recapitulated the clomipramine metabolism *in vivo*.

334 **3.5 Effects of clomipramine on the cardiac safety after its hepatic metabolism in**

335 **liver organoids**

336   Prior to examine the safety of clomipramine on cardiac tissues, we initially

337 evaluated the toxic effect of antidepressant on liver organoids. Clinically, the plasma

338 drug concentration of clomipramine in patients is 50 ∼ 600ng/ml (0.16-1.90 uM)[32] and

339 its active metabolite desmethylclomipramine exceeding a certain concentration (~1.43

340 μM) might lead to an increase in adverse reactions[33, 34]. Thus, the day-20 liver

341 organoids were exposed to a physiological relevant concentration of clomipramine (1

342 μM) and high dose of the drug (10 μM) for the treatment at different time periods (24

343 h and 48 h). As shown in **Fig. 6a**, liver organoids showed no significant changes of

344 cell viability after 1 μM clomipramine exposure compared to the control group, while

345 a decrease of cell viability with 10 μM clomipramine treatment for 48 h. Similarly,

346 the liver-specific functions, such as the urea synthesis in liver organoids was

347 markedly decreased with a high dose of clomipramine treatment **(Fig. 6b)**. These

348 results revealed that the high dose of clomipramine caused significantly damages of

349 cell viability and liver-specific functions, consisting with other reports or clinical

350 results.

351   To further explore the effects of clomipramine on the cardiac tissues following

352 liver metabolism, a low concentration of clomipramine (1 μM) was administered into

353 the integrated multi-organoids system. In this system, clomipramine and its

354 metabolites could diffuse to the bottom channel with cardiac organoids. After exposed

355 to 1 μM clomipramine for 24 h or 48 h in liver organoids, the cell viability of cardiac

356 organoids was initially examined to evaluate the drug-induced cardiotoxicity. The

357 data showed that clomipramine triggered significant cell death of cardiac organoids,

358 regardless of the presence or absence of liver organoids **(Fig. 6c)**. Moreover, the

359 effects of clomipramine administration on cardiac-specific functions, including the

360 beating rate and beating velocity of cardiac organoids were examined under different

361 culture conditions. The results showed that clomipramine can lead to reduced cardiac

362 beating rate and beating velocity from 20 μm/s to10 μm/s in the co-culture system

363 (**Fig. 6d-e**), indicating that the clomipramine-induced cardiotoxicity dependent on

364 liver metabolism. Calcium flux plays an important role in cardiac electrical activity

365 and directly activates the myofilaments, causing contractions. The concentration of

366 free intracellular Ca^{2+} oscillates during the cardiac action potential[35]. To monitor the

367 intracellular calcium influx, we used Fluo-4 AM to indicate the calcium handling of

368 cardiac organoids under different culture conditions. As shown in **Fig. 6f**, cardiac

369 organoids exhibited lower levels of cytosolic Ca^{2+} after treatment with 1 μM

370 clomipramine. Moreover, clomipramine could reduce the release of calcium flux in

371 cardiac tissue in co-culture systems, further proving the significant cardiotoxicity

372 induced by clomipramine metabolites. As we know, Tricyclic antidepressants (TCAs)

373 are highly lipid soluble drugs, which can pass through placenta, accumulate in utero,

374 and cause congenital malformations of fetus. The proposed multi-organoids-on-a-chip

375 system may have the potential to integrate with the maternal-fetal barrier and probe

376 the effects of clomipramine and its metabolites on cardio-development in the future.

377 The pharmacokinetic-pharmacodynamic (PK-PD) analysis can be applied on this

378 system, which provides an important guideline for dosage selection and drug

379 assessment[36, 37].

380

381 **4. Conclusion**

382   Herein, we proposed a new multi-organoids-on-chip system from hiPSCs that

383 allowed to assess the safety of antidepressants on cardiac tissue following liver

384 metabolism. This device contained compartmentalized chambers enables the

385 differentiation and 3D co-culture of functional liver and heart organoids

386 simultaneously. In this model, the administration of antidepressant clomipramine at a

387 low concentration led to the increased cardiotoxicity in heart organoids after its

388 metabolism in liver organoids, including the decreased cell viability, cardiac

389 contractility and calcium flux in heart organoids. These results showed the hepatic

390 metabolism-dependent toxic responses of this drug in cardiac tissue, revealing the

391 feasibility of this human multi-organoids chip system for predicting the side effects of

392 this antidepressant drug.

393 This work provides the proof-of-concept to develop hiPSC-derived

394 multi-organoids-on-chip by combining developmental biology principle and

395 bioengineered technology. The human organoids chip system enables to mimic the

396 multiorgan physiology by 3D co-culture of liver and heart organoids and facilitates

397 the assessment of drug safety in a physiological relevant manner. It could reflect the

398 multiple process of drug metabolism and responses at the multi-organ level *in vitro*,

399 which provides a novel platform for drug effectiveness and toxicity assessment.

400 **Acknowledgement**

406   CAS (DICP I201934).

407   **Competing interests**

408   The authors declare no competing financial interests.

Lab on a Chip Accepted Manuscript

410   **References**

411   1.   P. Molero, J. A. Ramos-Quiroga, R. Martin-Santos, E. Calvo-Sanchez, L.

412   Gutierrez-Rojas and J. J. Meana, *CNS Drugs*, 2018, **32**, 411-420.

413   2.   A. Z. Antosik-Wojcinska, B. Stefanowski and L. Swiecicki, *Psychiatr Pol*, 2015, **49**,

414   1223-1239.

415   3.   S. D. Kim, G. Kang, J. M. Kim, J. H. Ryu, K. C. Kim, H. S. Kwon, K. H. Kim, H. K. Lee

416   and S. W. Song, *Journal of Pharmacological and Toxicological Methods*, 2017, **88**,

417   198-199.

418   4.   W. J. Crumb, Jr., J. Vicente, L. Johannesen and D. G. Strauss, *J Pharmacol Toxicol*

419   *Methods*, 2016, **81**, 251-262.

420   5.   J. E. B. J. D. o. t. F. S. Randles, 1947, **1**.

421   6.   V. B. Siramshetty, J. Nickel, C. Omieczynski, B. O. Gohlke, M. N. Drwal and R.

422   Preissner, *Nucleic Acids Res*, 2016, **44**, D1080-1086.

423   7.   M. B. Esch, T. L. King and M. L. Shuler, *Annual Review of Biomedical Engineering,*

424   *Vol 13*, 2011, **13**, 55-72.

425   8.   M. A. Lancaster and J. A. Knoblich, *Science*, 2014, **345**, 1247125.

426   9.   X. L. Yin, B. E. Mead, H. Safaee, R. Langer, J. M. Karp and O. Levy, *Cell Stem Cell*,

427   2016, **18**, 25-38.

428   10.   W. Y. Q., W. H., D. P.W., T. T. T., L. H. T., W. S., C. W. W. and Q. J. H., *ACS*

429   *biomaterials science & engineering*, 2020, **6**, 5734-5743.

430   11.   Y. J. Zhu, L. Wang, H. Yu, F. C. Yin, Y. Q. Wang, H. T. Liu, L. Jiang and J. H. Qin,

431   *Lab on a Chip*, 2017, **17**, 2941-2950.

432   12.   Y. Wang, L. Wang, Y. Zhu and J. Qin, *Lab Chip*, 2018, **18**, 851-860.

433   13.   H. Liu, Y. Wang, K. Cui, Y. Guo, X. Zhang and J. Qin, *Advanced Materials*, 2019, **31**.

434   14.   S. N. Bhatia and D. E. Ingber, *Nature Biotechnology*, 2014, **32**, 760-772.

435   15.   D. Huh, Y. S. Torisawa, G. A. Hamilton, H. J. Kim and D. E. Ingber, *Lab on a Chip*,

436   2012, **12**, 2156-2164.

437   16.   J. P. Wikswo, *Future Sci OA*, 2017, **3**, FSO163.

438   17.   Y. Wang, H. Wang, P. Deng, W. Chen, Y. Guo, T. Tao and J. Qin, *Lab Chip*, 2018, **18**,

439   3606-3616.

440   18.   T. Tao, Y. Wang, W. Chen, Z. Li, W. Su, Y. Guo, P. Deng and J. Qin, *Lab Chip*, 2019,

441   **19**, 948-958.

442   19.   S. D. Sie, J. M. B. Wennink, J. J. van Driel, A. G. W. te Winkel, K. Boer, G. Casteelen

443   and M. M. van Weissenbruch, *Archives of Disease in Childhood-Fetal and Neonatal*

444   *Edition*, 2012, **97**, F472-F476.

445   20.   K. A. Yonkers, K. L. Wisner, D. E. Stewart, T. F. Oberlander, D. L. Dell, N. Stotland, S.

446   Ramin, L. Chaudron and C. Lockwood, *General Hospital Psychiatry*, 2009, **31**,

447   403-413.

448   21.   Z. Li, L. Jiang, T. Tao, W. Su, Y. Guo, H. Yu and J. Qin, *Toxicol Res (Camb)*, 2017, **6**,

449   372-380.

450   22.   F. Yin, Y. Zhu, M. Zhang, H. Yu, W. Chen and J. Qin, *Toxicol In Vitro*, 2019, **54**,

451   105-113.

452   23.   Q. Wang, H. Yang, A. Bai, W. Jiang, X. Li, X. Wang, Y. Mao, C. Lu, R. Qian, F. Guo,

453   T. Ding, H. Chen, S. Chen, J. Zhang, C. Liu and N. Sun, *Biomaterials*, 2016, **105**,

454   52-65.

455   24.   F. C. Yin, Y. J. Zhu, Y. Q. Wang and J. H. Qin, *ACS Biomater. Sci. Eng.*, 2018, **4**,

456   1908-1915.

457   25.   X. Lian, J. Zhang, S. M. Azarin, K. Zhu, L. B. Hazeltine, X. Bao, C. Hsiao, T. J. Kamp

458   and S. P. Palecek, *Nat Protoc*, 2013, **8**, 162-175.

459   26.   N. Huebsch, P. Loskill, M. A. Mandegar, N. C. Marks, A. S. Sheehan, Z. Ma, A.

460   Mathur, T. N. Nguyen, J. C. Yoo, L. M. Judge, C. I. Spencer, A. C. Chukka, C. R.

461   Russell, P. L. So, B. R. Conklin and K. E. Healy, *Tissue Eng Part C Methods*, 2015,

462   **21**, 467-479.

463   27.   A. Mathur, P. Loskill, K. Shao, N. Huebsch, S. Hong, S. G. Marcus, N. Marks, M.

464   Mandegar, B. R. Conklin, L. P. Lee and K. E. Healy, *Sci Rep*, 2015, **5**, 8883.

465   28.   C. Xu, L. Wang, Y. Yu, F. Yin, X. Zhang, L. Jiang and J. Qin, *Biomater Sci*, 2017, **5**,

466   1810-1819.

467   29.   M. D. Bootman, K. Rietdorf, T. Collins, S. Walker and M. Sanderson, *Cold Spring*

468   *Harb Protoc*, 2013, **2013**, 83-99.

469   30.   C. Oleaga, A. Riu, S. Rothemund, A. Lavado, C. W. McAleer, C. J. Long, K. Persaud,

470   N. S. Narasimhan, M. Tran, J. Roles, C. A. Carmona-Moran, T. Sasserath, D. H.

471   Elbrecht, L. Kumanchik, L. R. Bridges, C. Martin, M. T. Schnepper, G. Ekman, M.

472   Jackson, Y. I. Wang, R. Note, J. Langer, S. Teissier and J. J. Hickman, *Biomaterials*,

473   2018, **182**, 176-190.

474   31.   M. Gex-Fabry, E. Haffen, G. Paintaud, P. Bizouard, D. Sechter, P. R. Bechtel and L.

475   P. Balant, *Therapeutic Drug Monitoring*, 2000, **22**, 701-711.

476   32.   P. G. J. ter Horst, J. H. Proost, J. P. Smit, M. T. Vries, L. de Jong-van de Berg and B.

477   Wilffert, *European Journal of Clinical Pharmacology*, 2015, **71**, 1493-1500.

478   33.   S. H. Preskorn and G. S. Jerkovich, *J Clin Psychopharmacol*, 1990, **10**, 88-95.

479   34.   A. Szegedi, H. Wetzel, M. Leal, S. Hartter and C. Hiemke, *J Clin Psychiatry*, 1996, **57**,

480   257-264.

481   35.   D. M. Bers, *Nature*, 2002, **415**.

482   36.   C. W. McAleer, A. Pointon, C. J. Long, R. L. Brighton, B. D. Wilkin, L. R. Bridges, N.

483   Narasimhan Sriram, K. Fabre, R. McDougall, V. P. Muse, J. T. Mettetal, A. Srivastava,

484   D. Williams, M. T. Schnepper, J. L. Roles, M. L. Shuler, J. J. Hickman and L. Ewart,

485   *Sci Rep*, 2019, **9**, 9619.

486   37.   J. H. Sung, C. Kam and M. L. Shuler, *Lab Chip*, 2010, **10**, 446-455.

487

1   **Figures and legends**

Side view of multi-organoids on chip derived from hiPSCs for drug assessment
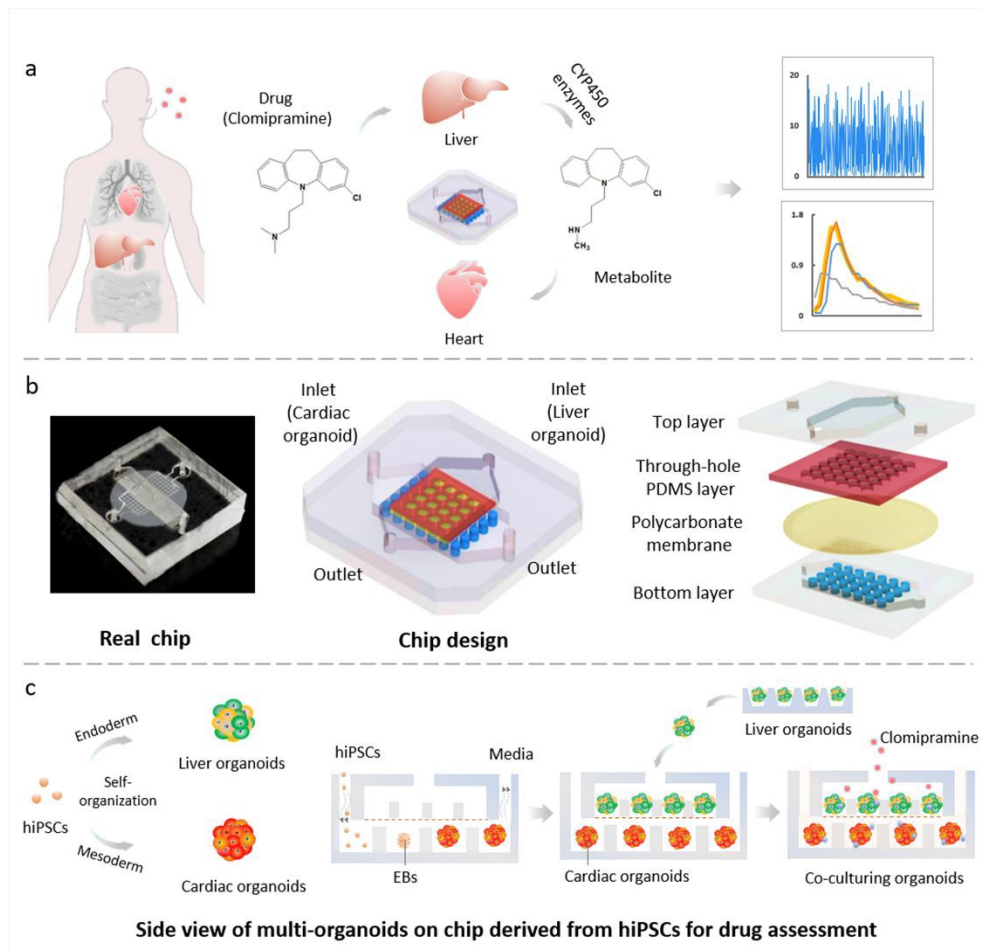
2

3   **Figure 1. Illustration of the liver-heart organoids-on-chip for drug assessment of**

4   **clomipramine. a,** Schematic diagram of antidepressant drug clomipramine and its

5   metabolites following liver metabolism *in vivo*. **b**, Design of multi-organoids-on-chip

6   device, which consists of the top layer, through-hole PDMS layer, polycarbonate

7   porous membrane and bottom layer. Self-organized liver organoids were cultured on

8   the upper through-hole PDMS layer to form liver region, and cardiac organoids were

9   cultured on the bottom micropillar layer to form heart region. **c,** The schematic

10   overview of the experimental procedures. Heart organoids were formed by in situ

11   differentiation and generation from hiPSCs on the bottom layer, and the day-20 hiPSC-

12   derived liver organoids were then seeded into the top layer, thereby establishing the co-

13   culture system of liver and heart organoids. Finally, this multi-organoids-on-chip was

14   applied to assess toxicity of antidepressant drug in heart organoids.

Lab on a Chip Accepted Manuscript

15
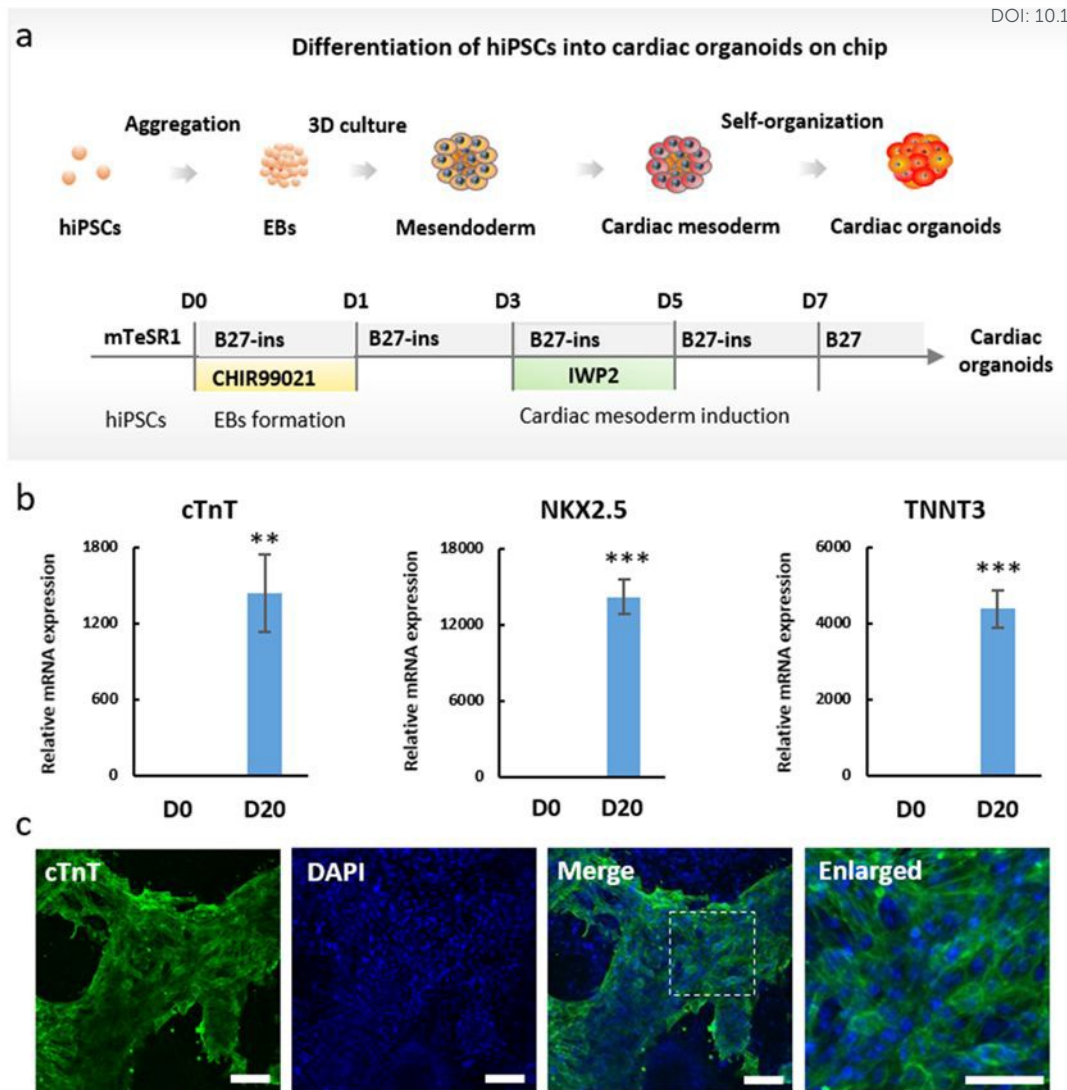
Figure 2. Characterization of hiPSC-derived cardiac organoids. a, The flow chart illustrates the process of the generation of heart organoids from hiPSCs. **b,** The relative mRNA expression of specific cardiac markers (cTnT, NKX 2.5, TNNT3) in day 20 cardiac organoids was quantified by real time-PCR, which were relative to that of day 0 hiPSCs. N=3 replicates, mean ± SD. (*, $P < 0.05$, **, $P < 0.01$, ***, $P < 0.001$). **c,** Immunohistochemistry analysis of cTnT in cardiac organoids on day 20. Scale bars, 100 μm.

23
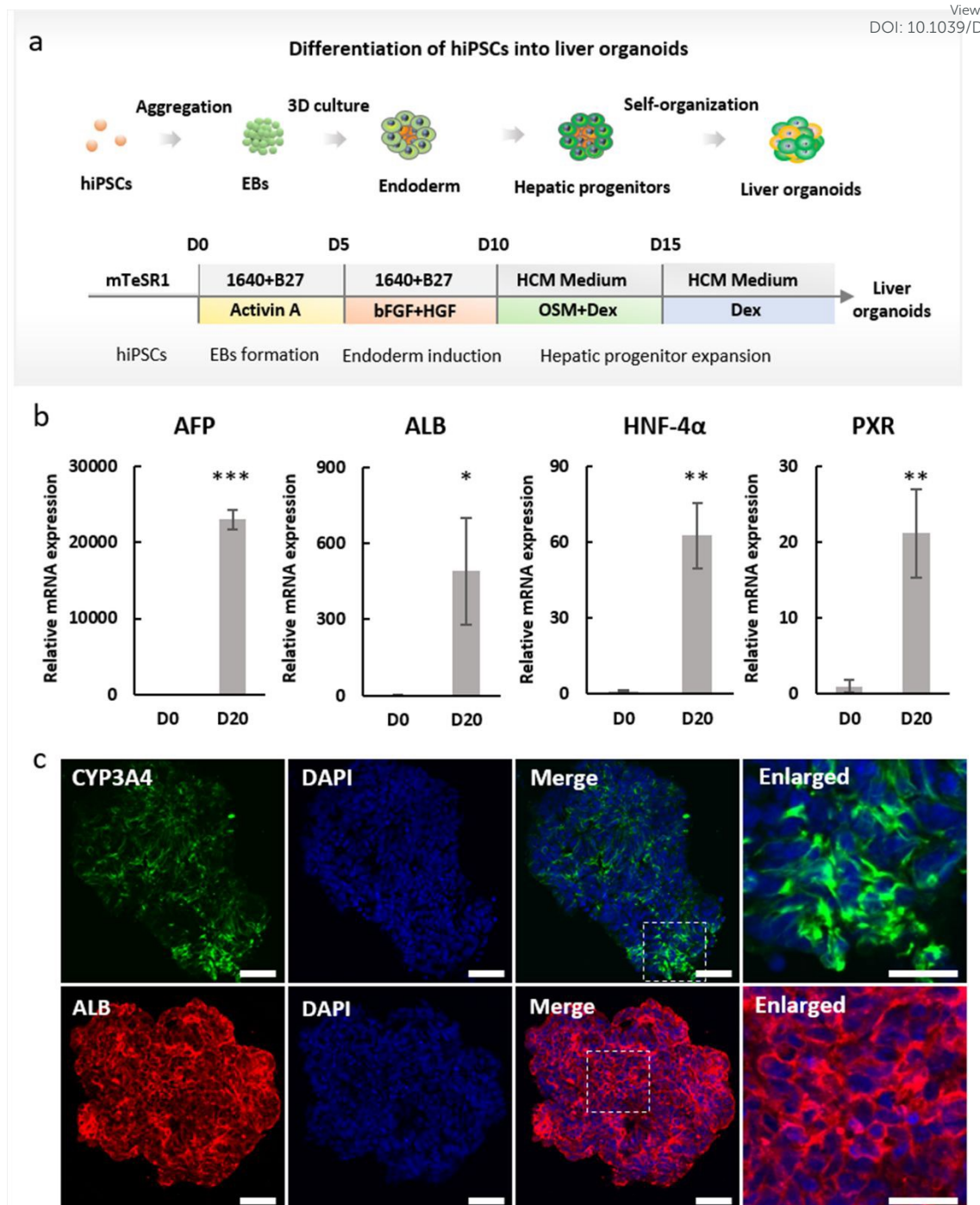
Figure 3. Characterization of hiPSC-derived liver organoids. a, The flow chart illustrates the process of the generation of hiPSC-derived liver organoids using a three-stage differentiation protocol. **b,** The hepatic progenitor (AFP), hepatocyte (ALB and HNF4α) and nuclear receptor (PXR) markers were quantified by real time-PCR in day 0 hiPSCs and day 20 liver organoids. N=3, mean ± SD. (*, $P < 0.05$, **, $P < 0.01$, ***, $P < 0.001$). **c,** Immunohistochemical staining of ALB and CYP450 enzyme marker (CYP3A4) in organoids on day 20. DAPI marks nuclei (blue). Scale bars, 50 μm.
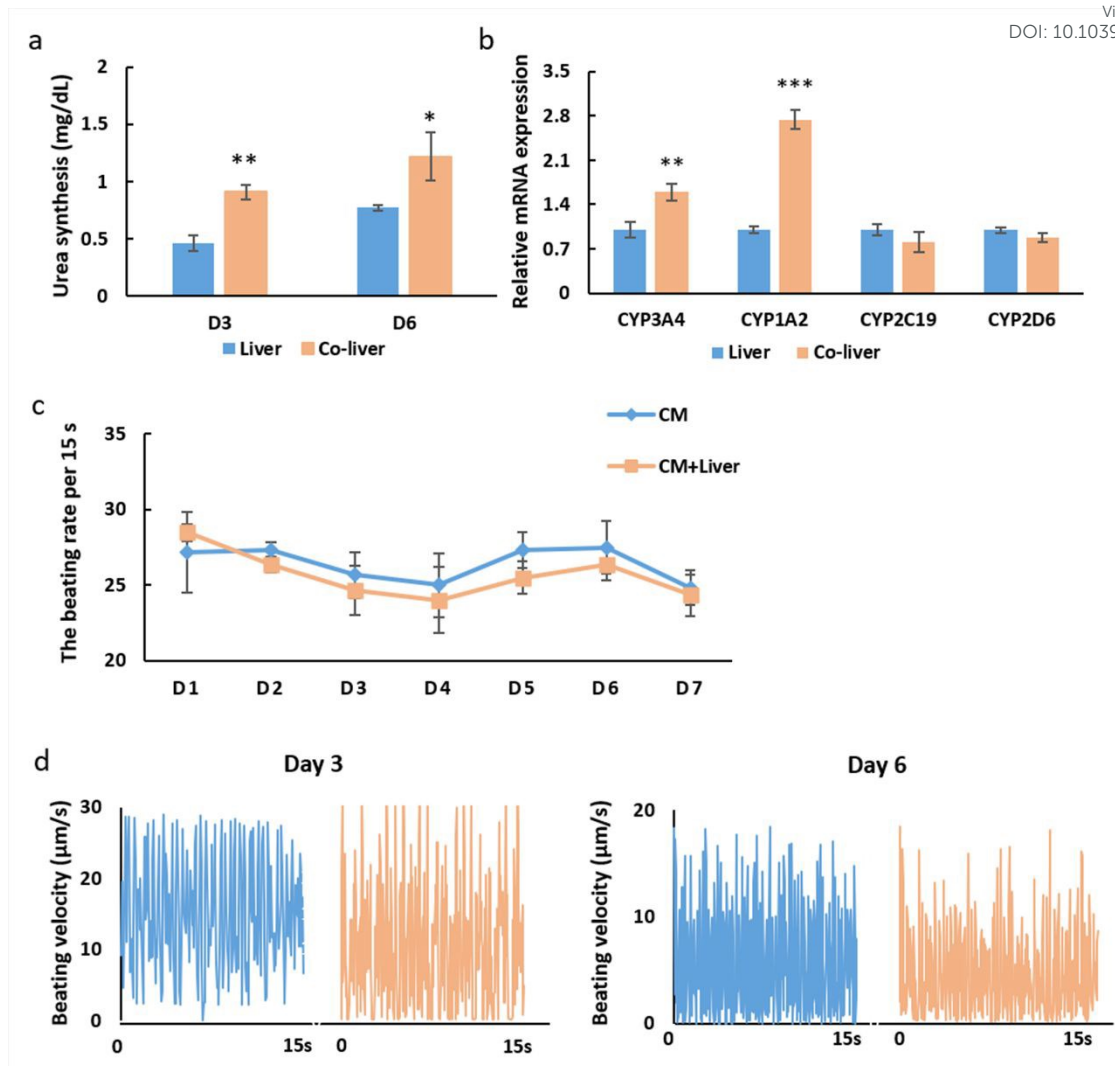
Figure 4. Characterization of the co-cultured human liver organoids and heart organoids on chip. a, Urea synthesis was quantified in liver organoids with (co-liver) or without (liver) cardiac tissues cultures on chip at 3 and 6 days. **b,** The mRNA expression of liver-specific metabolic enzymes (CYP3A4, CYP1A2, CYP2C19 and CYP2D6) in liver organoids with (co-liver) or without (liver) cardiac tissues coculture on chip was quantified by real time-PCR. N=3, mean ± SD. (*, $P < 0.05$, **, $P < 0.01$, ***, $P < 0.001$). **c-d,** Analysis of cardiac functional parameters: beat frequency **(c)** and beating velocity (μm/s) **(d)** in the presence or absence of liver organoids at different time points.

42
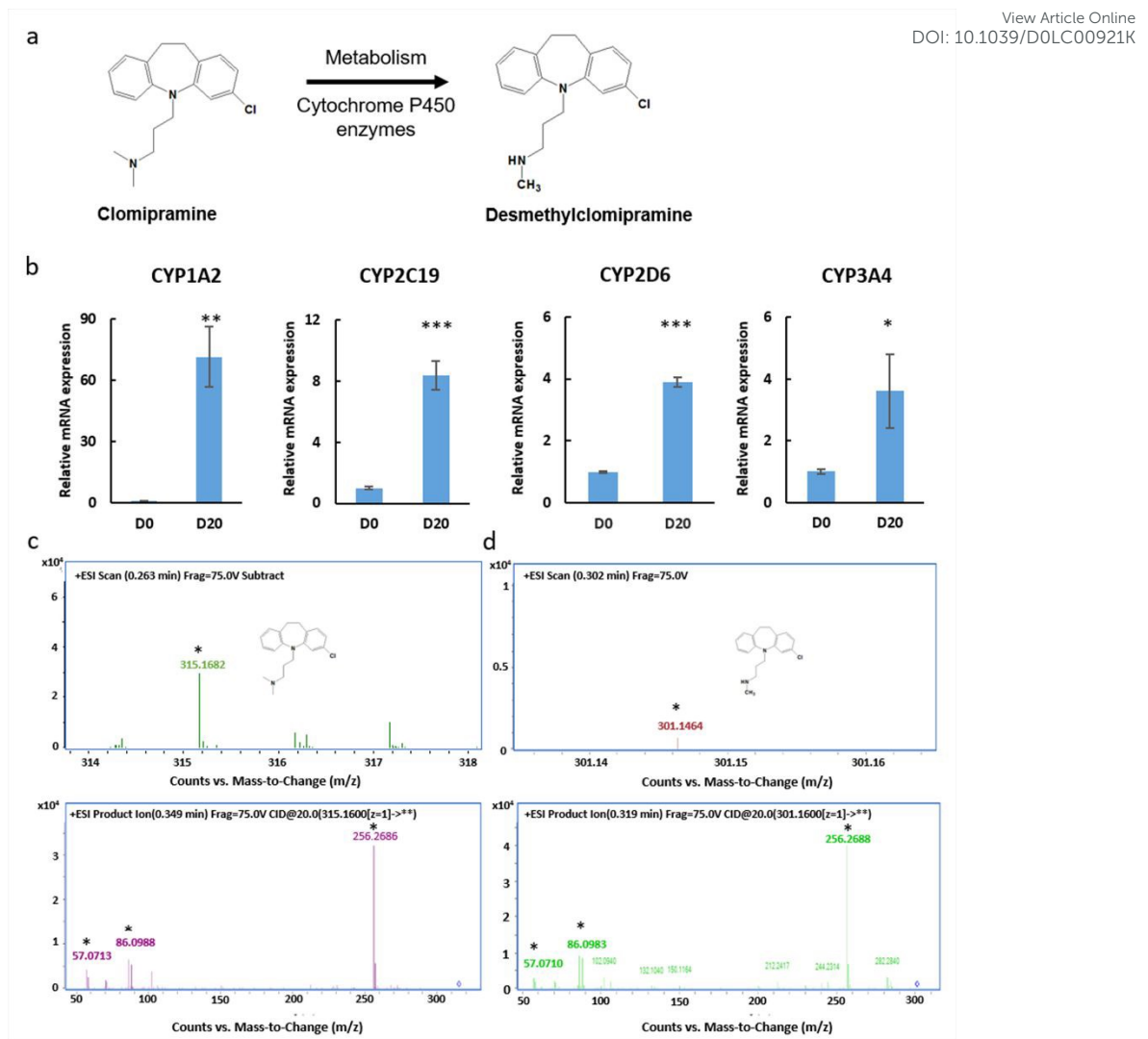
Figure 5. Identification of clomipramine and its metabolite (desmethylclomipramine) by liver organoids on the chip. a, The main metabolic process of clomipramine *in vivo*. **b,** The expression of metabolic enzyme genes (CYP1A2, CYP3A4, CYP2C19 and CYP2D6) were evaluated by real time-PCR in day 0 hiPSCs and day 20 liver organoids. N=3, mean ± SD. (*, $P < 0.05$, **, $P < 0.01$, ***, $P < 0.001$). **c-d**, Mass spectrum of clomipramine (**c**) and its metabolite (desmethylclomipramine) (**d**) (top) and the secondary mass spectrogram (bottom) from the supernatants of liver organoids with 1μM clomipramine treatment for 24 h using LC-MS (liquid chromatography mass spectrometry) technology.
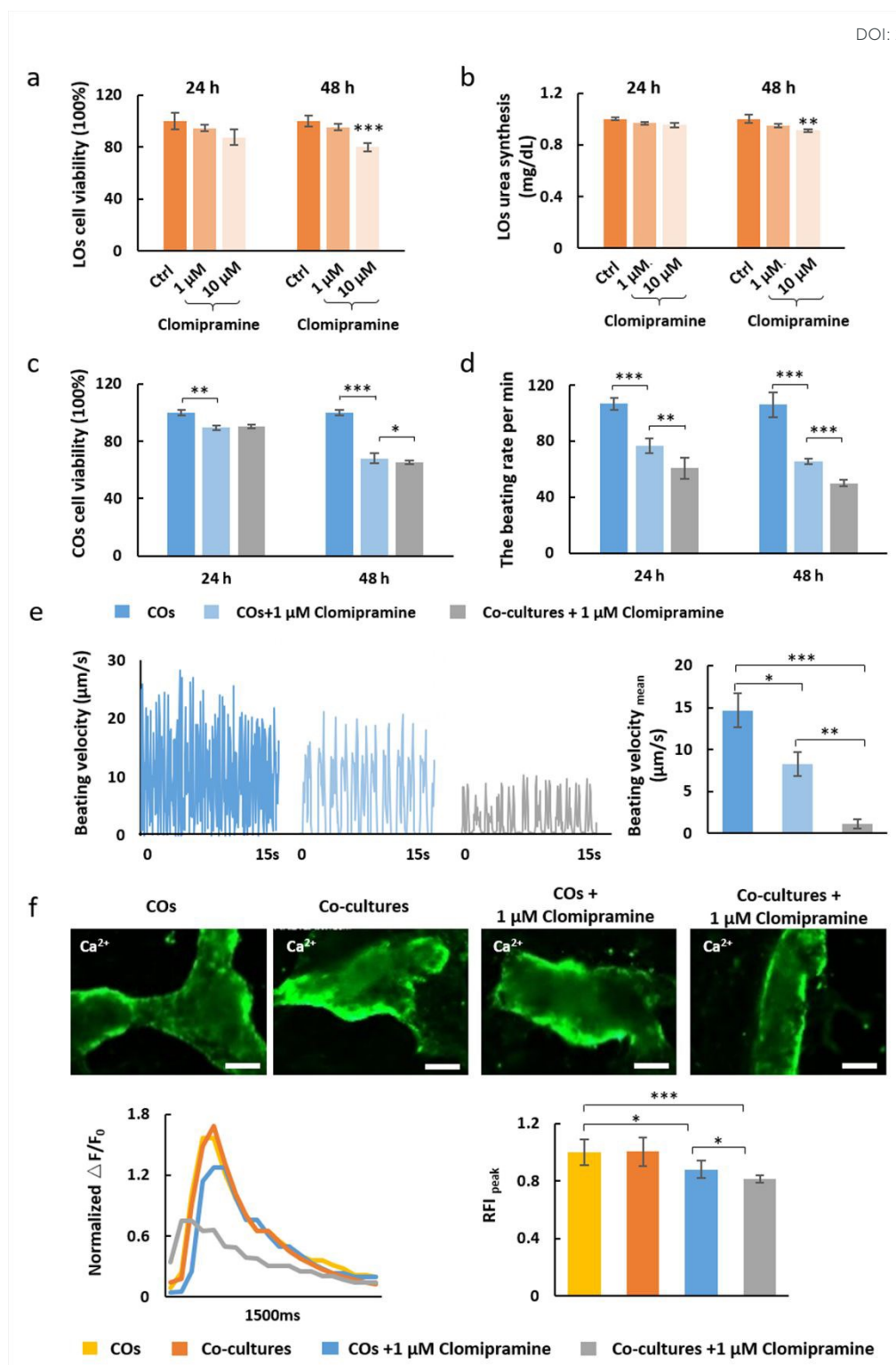
Figure 6. Assessment of drug-induced cardiactoxicity after liver metabolism on the liver-heart organoids-on-chip. a, Quantitative analysis of cell viability in liver organoids on day 20 after treatment with clomipramine (1 μM and 10 μM) for 24 and 48 h. The cell viability was analyzed using CCK-8 kit. **b,** Identification of the urea synthesis in liver organoids after treatment with different concentrations of

58   clomipramine for 24 and 48 h. N=3, mean ± SD. **c-d,** Cell viability (**c**) and the beating

59   rate (**d**) of the cardiac tissues were evaluated with clomipramine (1 μM) treatment for

60   24 h and 48 h in the presence and absence of liver organoids. N=3, mean ± SD. (*, $P <$

61   0.05, **, $P < 0.01$, ***, $P < 0.001$). **e,** Beating motion track of cardiac organoids with

62   different treatments and the quantification of mean beating velocity of each group (N=3,

63   mean ± SD. *, $P < 0.05$, **, $P < 0.01$, ***, $P < 0.001$). **f,** Fluorescence calcium imaging

64   of hiPSC-COs under different treatment conditions and the quantification of the peak

65   value of RFI. $\triangle F/F_0 = (F_t - F_0)/F_0$, where F_t was the fluorescent intensity values of each

66   frames and F_0 was the lowest fluorescence value. RFI: Relative fluorescence intensity.

67   Scale bars, 200 μm. (N=6, mean ± SD.*, $P < 0.05$, **, $P < 0.01$, ***, $P < 0.001$).